Variations of Particle Size Distribution, Black Carbon, and Brown Carbon during a Severe Winter Pollution Event over Xi'an, China

Qian Zhang[1,2,3], Zhenxing Shen[1,2]*, Yali Lei[1], Yueshe Wang[4], Yaling Zeng[1], Qiyuan Wang[2], Zhi Ning[3], Junji Cao[1], Linqing Wang[1], Hongmei Xu[1]

[1] Department of Environmental Science and Engineering, Xi'an Jiaotong University, Xi'an 710049, China
[2] Key Lab of Aerosol Chemistry & Physics, SKLLQG, Institute of Earth Environment, Chinese Academy of Sciences, Xi'an 710061, China
[3] School of Energy and Environment, City University of Hong Kong, Hong Kong, China
[4] State Key Laboratory of Multiphase Flow in Power Engineering, Xi'an Jiaotong University, Xi'an 710049, China

ABSTRACT

Real-time particulate matter (PM) size distributions, 4-hour time resolution, $PM_{2.5}$, carbonaceous materials, and their optical properties were measured during a severe pollution event in Xi'an, China. High $PM_{2.5}/PM_{10}$ ratios were observed on both pollution (0.83) and non-pollution (0.73) days, emphasizing the abundance of fine particles during sampling days. The particle number (PN) first peaked with a wide size range (30–100 nm) before morning rush hours (approximately 01:00–05:00) on pollution and non-pollution days, demonstrating that PN was governed by the accumulation of freshly emitted diesel particles and characterized by distinct aerosol condensation growth. By contrast, the second peak time and size range differed between pollution and non-pollution days because of different formation mechanisms. The light-absorbing coefficients of both black carbon (BC, $b_{abs-880nm,\ BC}$) and brown carbon (BrC, $b_{abs-370nm,\ BrC}$) were high on pollution days and decreased to approximately half of those values on non-pollution days, indicating that the degree of light absorption is reduced by rain. The diurnal variation in $b_{abs-880nm,\ BC}$ pollution peaked with traffic on January 1 and 2. By contrast, it remained in relatively stable and high ranges (120–160 Mm^{-1}) in the second period (January 3–5) without traffic peaks, illustrating that the dominant sources changed even during the same pollution period. High values of both $b_{abs-370nm,\ BrC}$ and $b_{abs-880nm,\ BC}$ coincided in the afternoon and evening due to emissions from primary sources, and abundant aqueous secondary organic carbon, respectively. A highly variable mass absorption coefficient of BrC also indicated the variety of fuel combustion sources of primary BrC in Xi'an.

Keywords: Severe pollution periods; Particle size distribution; Black carbon; Brown carbon.

INTRODUCTION

Urban pollution is an atmospheric phenomenon of high particulate matter (PM) loadings that leads to substantial visibility impairment at a relative humidity (RH) of less than 90% (Hyslop, 2009). Typically, the levels of PMs, including organic aerosol (OA) and black carbon (BC), and precursor gases increase substantially on pollution days (Odman *et al.*, 2009; Zheng *et al.*, 2015; Fang *et al.*, 2017). Severe pollution has attracted considerable scientific interest because of its effects on public health and climate change (Pope *et al.*, 2002; Nel, 2005; Law and Stohl, 2007; Peplow *et al.*, 2014; Von Schneidemesser *et al.*, 2015). Given the effect of urban air pollution, most studies have focused on

examining the concentrations and chemical compositions of gaseous pollutants and PMs. However, studies have confirmed that PM size is a key indicator of particle formation and growth (Ketzel *et al.*, 2004; Liu *et al.*, 2008; Yue *et al.*, 2016). Hitchins *et al.* (2000) indicated that 50% of total particle number (PN) concentrations in the 20–500-nm range decreased with an increase in distance from pollution sources. Different size distributions were found in PM chemical species and can be used to classify the sources and variations of particles with the PN (Liu *et al.*, 2008; Ma *et al.*, 2012; Tian *et al.*, 2014). For instance, both nucleation and Aitken mode particles (3–130 nm) indicate fresh emissions, such as emissions from gasoline and diesel engines (Zhang and Wexler, 2004; Shi *et al.*, 2010), whereas accumulation mode and larger particles mainly form from a series of chemical transformations (Zhang *et al.*, 2004). Thus, investigating how particle size and number change during pollution periods can be beneficial.

Current climate models and field studies indicate that

---

* Corresponding author.

E-mail address: zxshen@mail.xjtu.edu.cn

aerosol light absorption is a critical component in climate forcing (Bond and Bergstrom, 2006), because light-absorbing carbonaceous (LAC) particles are not only the essential components of PM (Ramanathan and Carmichael, 2008) but also the dominant absorbers of solar radiation in the atmosphere. In airborne carbonaceous species, two types of LACs are present: BC (at visible and infrared wavelengths) and brown carbon (BrC; at near-ultraviolet wavelengths). Both change Earth's radiative balance and drastically reduce visibility. Primary or pure BC exhibits a graphite-like structure with small-sized (10–50 nm) spherules and is a primary pollutant with high chemical stability emitted mainly from internal combustion (Wentzel *et al.*, 2003; Guha *et al.*, 2015; Sarkar *et al.*, 2015). However, pure BC is rarely found in the atmosphere and agglomerates rapidly after emission by adsorbing organic and inorganic vapors through typical aging processes. This leads to complex physical and light absorption properties (Kotzick and Niessner, 1999; Levitt *et al.*, 2007; Liu and Smallwood, 2011; Lin *et al.*, 2016; Zhan *et al.*, 2016; Zhou *et al.*, 2018). BC and BrC have entirely different morphologies, optical and chemical properties, and emission sources. In contrast to BC, BrC is large with a diameter of 100–400 nm, and its fraction may contain hundreds of organic compounds with varying atmospheric behaviors (Andreae and Gelencsér, 2006; Alexander *et al.*, 2008).

Xi'an (34°16′N, 108°54′E, 400-m above sea level) is a megacity located in the center of Northwest China with a population density of 870 per km^2. Because of its geographical location in the Guanzhong Plain, Xi'an is surrounded by the Qinling Mountains in south and the Loess Plateau in north and experiences frequently stagnant conditions; the city's air pollution can be easily trapped and exacerbated (Shen *et al.*, 2009, 2014). According to atmospheric visibility data, airborne emissions in Xi'an have decreased over the last 10 years (Shen *et al.*, 2016); however, winter pollution remains severe. In this study, a high-resolution analysis of particle size distribution, gas precursors, PM levels, and their carbon species was conducted. In addition, aerosol properties, such as concentration, size distribution, and light absorption, were characterized and compared between pollution and non-pollution days.

METHODOLOGY

Observational Site

We performed field observations in a representative site in the southeast area of downtown Xi'an (34°16′N, 108°54′E; Fig. 1). Both online and offline instruments were located on a rooftop (approximately 15-m high) at Xi'an Jiaotong University that is exposed to complex emission sources (Shen *et al.*, 2012; Zhang *et al.*, 2015). Residential areas and the campus of Xi'an Jiaotong University are to the north and east, respectively. Two heavily used roads, the South Second Ring Road and Xingqing Road, are to the south and west, respectively. Many diesel-powered trucks and buses ply on these roadways at night.

Fig. 1. Sampling site.

Xi'an, as well as other cities in northern China, experienced heavy pollution in winter in recent years and suffered through the longest stretch of stifling air pollution ever recorded in the country. The poor-quality air during this stretch consisted of exceedingly high concentrations of particles less than 2.5 μm in diameter (PM$_{2.5}$, surpassed 500 μg m^{-3}), and this stretch ended through precipitation and high winds 1 week later. According to the ambient air quality standards (AAQS) of China (GB3095-2012: http://kjs.mep.gov.cn/hjbhbz/bzwb/dqhjbh/qhjzlbz/201203/t20120302 _224165.htm) and the measured data in this study, pollution day was defined as that the 24-h average concentrations of both PM$_{2.5}$ and PM$_{10}$ were twice times higher than the national AAQS-Grade II value (PM$_{2.5}$, 75 μg m^{-3}; PM$_{10}$, 150 μg·m^{-3}). In this study, two episodes are identified and discussed during our sampling days: January 1–5, 2017 (pollution days), and January 6, 2017 (non-pollution day).

Time-integrated PM$_{2.5}$ Collection and Carbonaceous Species Analysis

A total of 42 PM$_{2.5}$ samples with time resolution of 4 hours were collected on Whatman 47 quartz filters (Whatman Inc., Maidstone, UK) by using a PQ200 ambient air particulate sampler (BGI Inc., USA) at a flow rate of 16.7 L min^{-1}. The filter samples were equilibrated for 24 hours at 20–23°C in a chamber at relative humidity (RH) of 35% and 45% before and after sample collection, respectively. They were weighed at least three times on a high-precision (± 1 μg) microbalance (ME-5, Sartorius Inc., Germany) to determine PM mass. After weighing, all the samples were stored in a freezer at approximately 20°C to prevent the evaporation of volatile compounds until analysis (Shen *et al.*, 2010).

A 0.5-cm^2 punch of each sample was analyzed for elemental carbon (EC) and organic carbon (OC) of PM$_{2.5}$ following the Interagency Monitoring of Protected Visual Environments thermal and optical reflectance protocol by using a DRI Model 2001 thermal and optical carbon analyzer (Atmoslytic Inc., California, USA). OC fractions (OC1, OC2, OC3, and OC4 at 120°C, 250°C, 450°C, and 550°C, respectively, in a helium atmosphere) and EC fractions (EC1, EC2, and EC3 at 550°C, 700°C, and 800°C, respectively, in 2% oxygen and 98% helium) were also collected. During volatilization of OC, a part of the OC was converted pyrolytically to EC (this fraction of OC was called OP) (Chow *et al.*, 2005). Therefore, OC is the sum of OC1, OC2, OC3, OC4, and OP, and EC is the sum of EC1, EC2, and EC3 minus OP. Additional quality assurance procedures are described in detail by Cao *et al.* (2005).

Collection of Particle Size Distribution Data

The size distribution (18.1–532.5 nm) and concentration of aerosol particles were continuously monitored using a scanning mobility particle sizer (SMPS) during sampling periods. The SMPS consists of a single-stage impactor (with a cutoff diameter of 0.5–0.7 μm), a differential mobility analyzer (Model 3082), and a condensation particle counter (Model 3775). These particle sizers are routinely used to

accurately measure sizes of nanoparticles suspended in liquids. The aerosol flow rate of 3.3 L min^{-1} was carefully selected to be sufficiently high to remove large particles from aerosols in the impactor but sufficiently low to provide the residence time necessary to measure and separate particles. This time consisted of a 30-s scan, 6-s retrace, and 10-s purge (Chen *et al.*, 2016). A more detailed description of the SMPS is provided by Gulijk *et al.* (2004).

BC and BrC Measurements

The concentration and optical parameters of BC were determined using a seven-wavelength Aethalometer-31 (Model-AE31, Magee Scientific Inc., USA). The flow rate of AE31 was calibrated prior to deployment. The sampling air flow rate was 5.0 L min^{-1}. AE31 was programmed to automatically determine aerosol light absorption at seven wavelengths (370, 470, 520, 590, 660, 880, and 950 nm) in μg m^{-3} at 5-min intervals over the sampling period from a location near PM$_{2.5}$ samplers. The accuracy of data from AE31 is affected by two factors: a nonlinear response as loading levels on the filter media increase (loading factor) and the effects of light scattering by fiber filter substrates (Collaud Coen *et al.*, 2010). These factors were considered and corrected in the study of Shen *et al.* (2017).

The light absorption coefficient (b_{abs}) is the most important parameter for BC and BrC determination. The absorption at 880 nm is assumed to be contributed only by BC, whereas absorption at a lower wavelength (370 nm) is assumed to be contributed by both BC and BrC. Therefore, b_{abs} at 880 nm refers to $b_{abs-880nm, BC}$. The BrC absorption was derived from the filter-based aerosol absorption spectrum analysis by subtracting BC absorption (Olson *et al.*, 2015). First, we projected the absorption coefficient (b_{abs}) of BC at 880 nm to full spectrum (370, 470, 520, 590, 660, 880, 950 nm) using AAE = 1. Then, the $b_{abs-370nm, BC}$ is subtracted from the b_{abs} values at 370 nm ($b_{abs-370nm}$) to estimate the $b_{abs-370nm, BrC}$. The detailed descriptions can be found in Olson *et al.* (2015) and Zhang *et al.* (2017).

The value of Absorption Ångström exponent (AAE), referred to as a power exponent of wavelength, is nearly constant (~1) for BC but is 1.2 or much higher for BrC. The relationship between wavelength-dependent AAE and b_{abs} of BC and BrC were described as: $b_{abs} = K \times \lambda^{-AAE}$ (here K refers to a constant value and λ denotes wavelength of BrC), and the AAE$_{Full spectrum}$ was determined by statistical regression fitting the b_{abs} data covering the UV to the near-IR ranges (includes 370, 470, 520, 590, 660, 880, and 950 nm) with a power law equation.

The mass absorption coefficient (MAC) is a primary parameter used to characterize the optical properties of BC. The MAC can build the relationship between optical properties and mass concentrations of BC and is expressed in m^2 g^{-1}. All BC data were normalized with EC data from the same station to produce EC-equivalent BC values. BC calculation used site-specific MAC values. The MAC-BrC (for aqueous BrC) was calculated by dividing $b_{abs-370nm, BrC}$ by the OC filter-based concentration (Olson *et al.*, 2015). We can calculate MAC-BrC and MAC-BC using the following equations:

$$\text{MAC-BrC} = b_{abs\text{-}370nm,\ BrC}\ (\text{Mm}^{-1})/\text{OC}\ (\mu\text{gm}^{-3}) \qquad (1)$$

$$\text{MAC-BC} = b_{abs\text{-}880nm,\ BC}\ (\text{Mm}^{-1})/\text{EC}\ (\mu\text{gm}^{-3}) \qquad (2)$$

Both EC and OC were obtained from the DRI Model 2001 thermal and optical carbon analyzer mentioned in section 2.2.

Online Aerosol, Trace Gases, and Meteorology Measurement

Hourly concentrations of nitrogen dioxide (NO_2), sulfur dioxide (SO_2), and ozone (O_3) gases and time-integrated $PM_{2.5}$ and PM_{10} were collected from the data center of the Ministry of Environmental Protection of China (http://datacente r.mep.gov.cn). Meteorological parameters, including temperature, RH, visibility, and wind speed/direction (WS/WD), were obtained from the Shaanxi Meteorological Bureau at the "Xingqing residential area" meteorological station located approximately 3 km north of the sampling site.

RESULTS AND DISCUSSION

Brief Introduction of Severe Pollution Days

The daily average PM level, along with the meteorological parameters (temperature, RH, WS, and visibility), between January 1, 2017, and January 6, 2017, are listed in Table 1. The daily mean visibility on pollution days ranged from 1.1 to 1.6 km and improved to 3.1 km on non-pollution days. The visibility in Xi'an was still much lower than that in other Chinese megacities during winter pollution periods (e.g., 3.3 km in Guangzhou (Tan *et al.*, 2009) and 2.6 km in Beijing (Yang *et al.*, 2015)), confirming that this pollution period was particularly severe. Fig. 2 depicts two peaks of diurnal variations of visibility observed during the sampling periods. The first peak was 3 km in the early morning of January 2, and this peak was heavily influenced by the wind which originated from northeastern directions (WD: 30–80°) was high (> 3.5 m s^{-1}, Fig. 2). The second peak was 3.5 km in the afternoon of January 5 and was mainly caused by the appearance of wet depositions, the rising PBL, and high WS (> 4 m s^{-1}) from northeastern direction (WD: 40–90°).

On pollution days, the average concentrations of $PM_{2.5}$ and PM_{10} were 396.2 and 476.7 µg m^{-3}, respectively; these were 5.2 and 3.2 times higher than the Chinese National

Ambient Air Quality Standard (GB3095-2012) of 75 for $PM_{2.5}$ and 150 µg m^{-3} for PM_{10} (An *et al.*, 2013). Low WS values (< 2 m s^{-1}) indicated that high PM loadings were accompanied by poor diffusion conditions. High PM levels always corresponded to low visibility under a high RH (approximately 86%), implying that the hygroscopic growth of PM-soluble components leads to substantial visibility degradation (Cheng *et al.*, 2013; Liu *et al.*, 2013). By contrast, the mean levels of $PM_{2.5}$ and PM_{10} on non-pollution days were only half of those on pollution days. The mean $PM_{2.5}/PM_{10}$ ratio remained high on both pollution and non-pollution days (0.83 vs. 0.73), indicating that airborne particles were mainly present as $PM_{2.5}$ during sampling days (Fig. 3(a)).

The average mass concentration of SO_2 on pollution days was 43.4 µg m^{-3}, which was 1.6 times higher than that on non-pollution days. The mean concentrations of typical vehicle emissions, namely NO_2, carbon monoxide (CO), and BC, were 111.7, 4089, and 13.7 µg m^{-3} on pollution days compared with 53.1, 3277, and 7.8 µg m^{-3} on non-pollution days. Meanwhile, these traffic markers showed similar diurnal patterns on pollution days, peaking during the heavily polluted time periods of morning (09:00–11:00) and evening (19:00–21:00) rush hours. After rain (05:00), the concentrations of NO_2, CO, and BC rapidly decreased on January 6; however, the concentration of BC declined faster than that of CO, indicating that BC in Xi'an was coated by more hydrophilic groups and was more susceptible to wet depositions near the end of the heavy pollution (Dalirian *et al.*, 2017). The O_3 concentration showed large daily variability, varying from 5.3 to 22.4 µg m^{-3} with an average value of 14.2 µg m^{-3}; however, it remained lower than that during other seasons (Wang *et al.*, 2012), indicating weak atmospheric oxidation capacity on pollution days.

Number and Size Distribution

Fig. 4 shows the comparison of size distributions (ranging from 18.5 to 532.5 nm) and mean concentrations between pollution and non-pollution days in Xi'an. The number of pollution particles peaked at 50–70 nm and can be identified as Aitken mode particles, which are slightly larger than the size of freshly emitted particles (approximately 30 nm), emphasizing that PM pollution was heavily influenced by fresh emissions and grew under stable atmospheric conditions (Zhang *et al.*, 2017). The mode of non-pollution particles was between 100 and 170 nm, and half of them were in the

Table 1. Meteorological parameters and online PM concentrations during sampling days.

| Date		Meteorological conditions				PM mass concentrations		
		Visibility/km	RH/%	WS/m s^{-1}	Temp/°C	$PM_{2.5}$/µg m^{-3}	PM_{10}/µg m^{-3}	$PM_{2.5}/PM_{10}$
Pollution days	1 Jan	1.5 ± 0.2	77.3 ± 13.3	1.6 ± 0.7	1.7 ± 2.9	350. 7 ± 36.1	416.9 ± 42.2	0.84
	2 Jan	1.6 ± 0.6	82.5 ± 20.8	1.8 ± 0.9	0.6 ± 4.6	305.3 ± 42.6	377.8 ± 44.5	0.81
	3 Jan	1.3 ± 0.2	87.2 ± 15.5	1.4 ± 0.5	0.5 ± 4.8	364.9 ± 41.9	441.1 ± 50.8	0.83
	4 Jan	1.1 ± 0.1	82.9 ± 17.8	1.3 ± 0.5	2.3 ± 3.3	468.4 ± 46.9	556.1 ± 51.9	0.84
	5 Jan	1.6 ± 0.8	87.6 ± 7.1	1.9 ± 0.9	1.9 ± 3.3	491.8 ± 54.5	591.4 ± 60.8	0.83
	Average	1.4 ± 0.2	84.1 ± 4.9	1.6 ± 0.2	1.5 ± 0.8	396.2 ± 71.6	476.7 ± 82.6	0.83
Non-pollution day	6 Jan	3.1 ± 0.5	95.6 ± 6.0	2.6 ± 1.6	3.3 ± 0.7	174.0 ± 106.3	239.8 ± 137.9	0.73

WS refers to wind speed; Temp refers to temperature; PM refers to particulate matter.
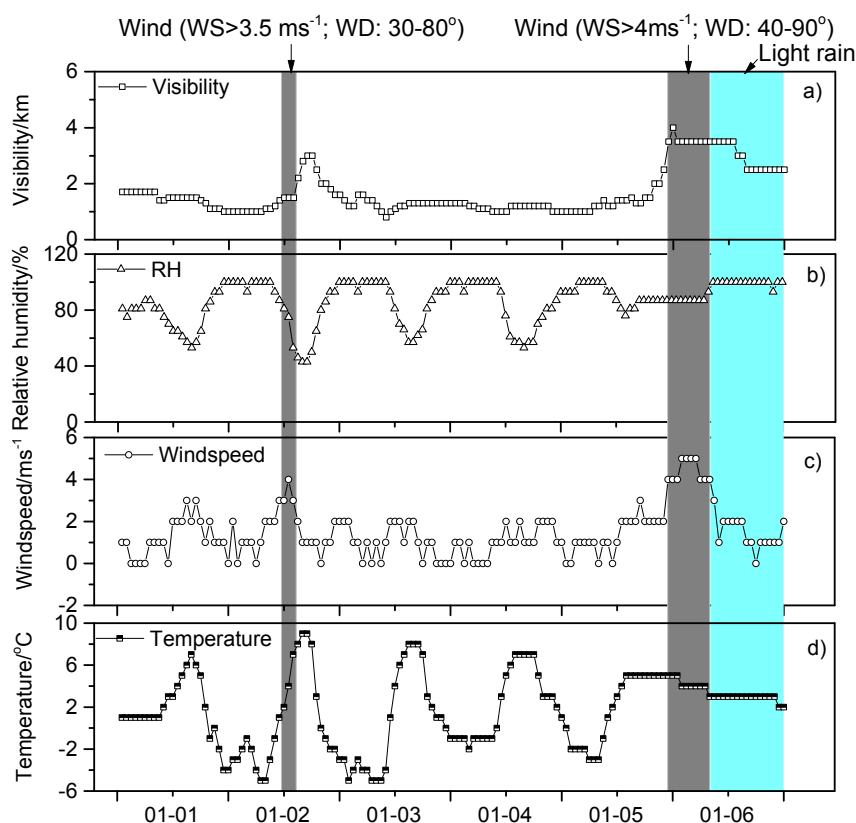
Fig. 2. Temporal variations of meteorological parameters with time resolution of 1 h during a severe pollution period in Xi'an. (a) Visibility; (b) RH; (c) Wind speed and (d) Temperature.
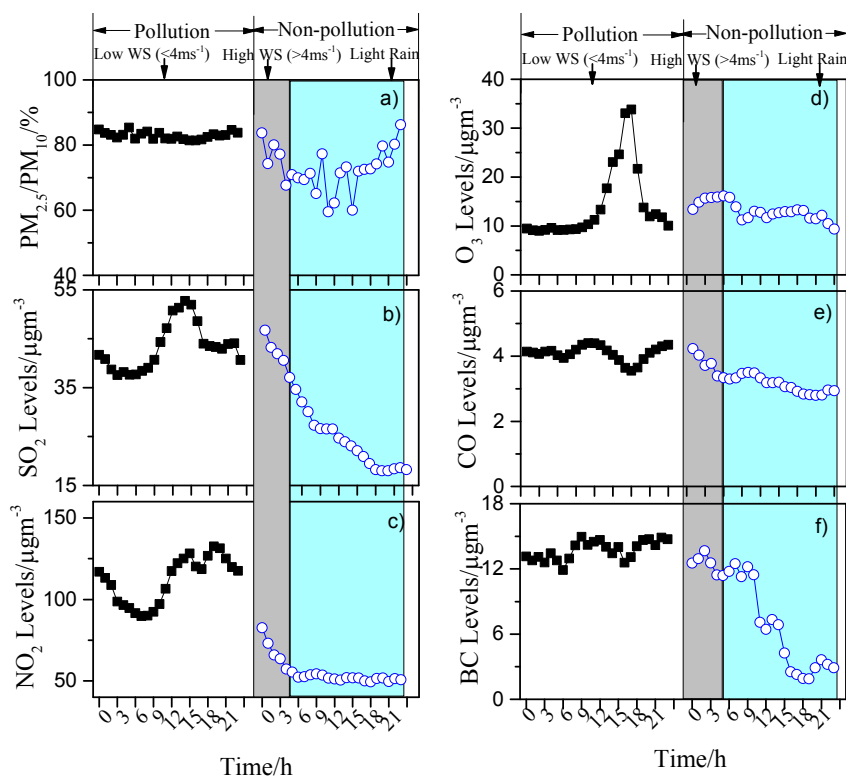
Fig. 3. Time series of $PM_{2.5}$/ PM_{10} ratios and gaseous pollutants with time resolution of 1 h for pollution and non-pollution days in Xi'an. (a) $PM_{2.5}$/PM_{10} ratios; (b) SO_2 mass concentration; (c) NO_2 mass concentration; (d) O_3 mass concentration; (e) CO mass concentration; (f) BC mass concentration. (WS: wind speed).
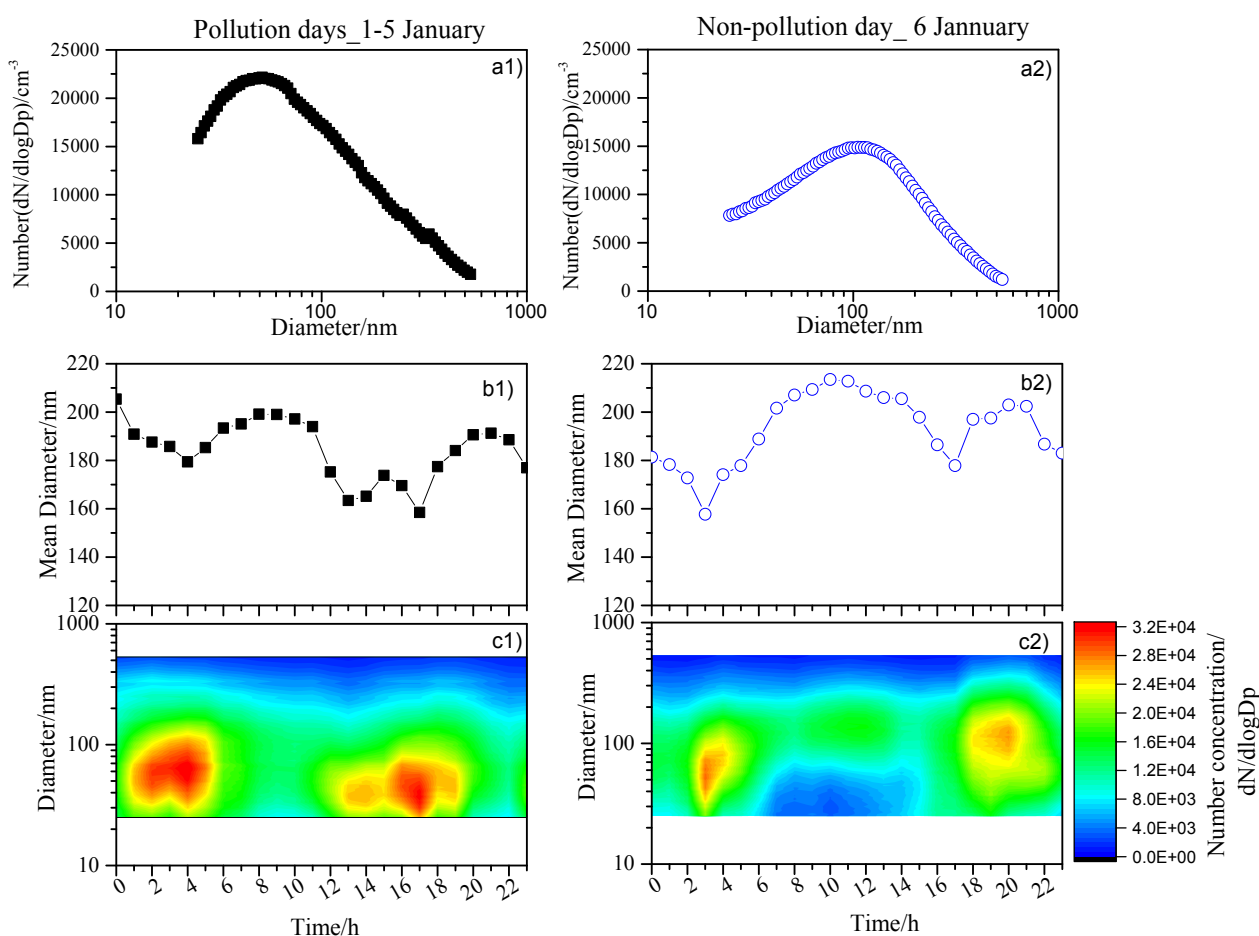
Fig. 4. Comparison of measurements between pollution and non-pollution days: (a) Particle size distribution, the solid lines represent lognormal fits; (b) Time series of mean diameter; (c) Diurnal variations of mean number concentrations (*dN/dlogDp*).

range of the accumulation mode (130–1000 nm), attributing to the growth of non-pollution particles through condensation and coagulation (Bukowiecki *et al.*, 2002; Liu *et al.*, 2008; Polidori *et al.*, 2008). The mean diameter of pollution particles was slightly smaller than that of non-pollution particles, confirming that a high RH contributes to the growth of particles (Winkler, 1973).

During pollution days, diurnal PN concentrations peaked before morning rush hours (approximately 01:00–05:00) at a wider size range (30–100 nm) mainly because of the accumulation of freshly emitted particles and the condensation growth of new particles from diesel vehicles. This demonstrated that freshly emitted diesel particles during this time contributed substantially to the abundant PN at fixed size range (around 100 nm), providing some justification for the "Government Strengthening Management on Vehicle Exhaust" in Xi'an. During the second peak of pollution PN, both Aitken and accumulation modes were observed in the afternoon (15:00–18:00). This peak was not coincided with the variations of fresh vehicle emissions such as CO, NO_2, and BC. In fact, low O_3 level implied the weak atmospheric oxidation. Therefore, this peak should mainly form from the condensation process under the conditions of relatively highly pre-existing PM levels

(Maricq, 2007; Gao *et al.*, 2009; Perez *et al.*, 2010).

The diurnal patterns of non-pollution PN distribution were also observed in Fig. 4(b2). The two peaks occurred during early morning (02:00–04:00) and evening rush hours (18:00–20:00). In the first peak, the size range was similar to pollution particles, but the time interval of the PN was shorter. By contrast, the evening peak of non-pollution PM was different from that of pollution PM and appeared at a larger size range (80–200 nm). This was caused by the rapid growth of intensive traffic particles and condensation mechanisms under a high RH (Zhang *et al.*, 2017).

### Time-integrated Offline PM₂.₅ Carbonaceous Concentrations

The total carbon (TC) concentration was calculated as 40.8 µg m⁻³ on pollution days and 17.2 µg m⁻³ on non-pollution days. TC, which includes EC and OC, constitutes a substantial fraction of $PM_{2.5}$ mass (24.4% on pollution days and 23.1% on non-pollution days) and heavily influences ambient optical properties (Andreae and Gelencsér, 2006; Bond and Bergstrom, 2006). The variations of TC/$PM_{2.5}$ changed slightly during sampling days (Fig. 5(a)). These phenomena emphasized that carbon materials were key

constituents of $PM_{2.5}$, and their sources appeared to be stable during sampling days. A strong correlation ($R = 0.8$, $P < 0.001$) was observed between OC and EC, indicating that TC maintains a fairly constant level as a primary pollutant in Xi'an (Cao *et al.*, 2007). The time-integrated percentages of the eight carbon fractions are listed in Fig. 5(b). During sampling days, EC1, OC3, and OC4 were the most abundant carbon fractions and contributed approximately 60% of TC. This emphasizes the contribution from coal burning (Cao *et al.*, 2005; Shen *et al.*, 2010). The abundance of gasoline emissions led to high levels of OC1 and OC2, but low EC2 and EC3 indicated fewer diesel

emissions. Additionally, the OC/EC ratios in this study varied from 3.0 to 5.8, indicating the presence of secondary organic carbon (SOC) (Zhang *et al.*, 2015, 2017). In addition, the substantial OC2 and OC3 concentrations were always associated with SOC (Gu *et al.*, 2010). SOC concentration was estimated based on the EC-tracer method in Turpin and Huntzicker (1995). Thus, the estimation of SOC occupied approximately 30% of OC during severe pollution periods.

Characteristics of LAC Optical Properties

Earlier studies have defined LACs as pure LAC aerosols that include the strongly light-absorbing refractory BC
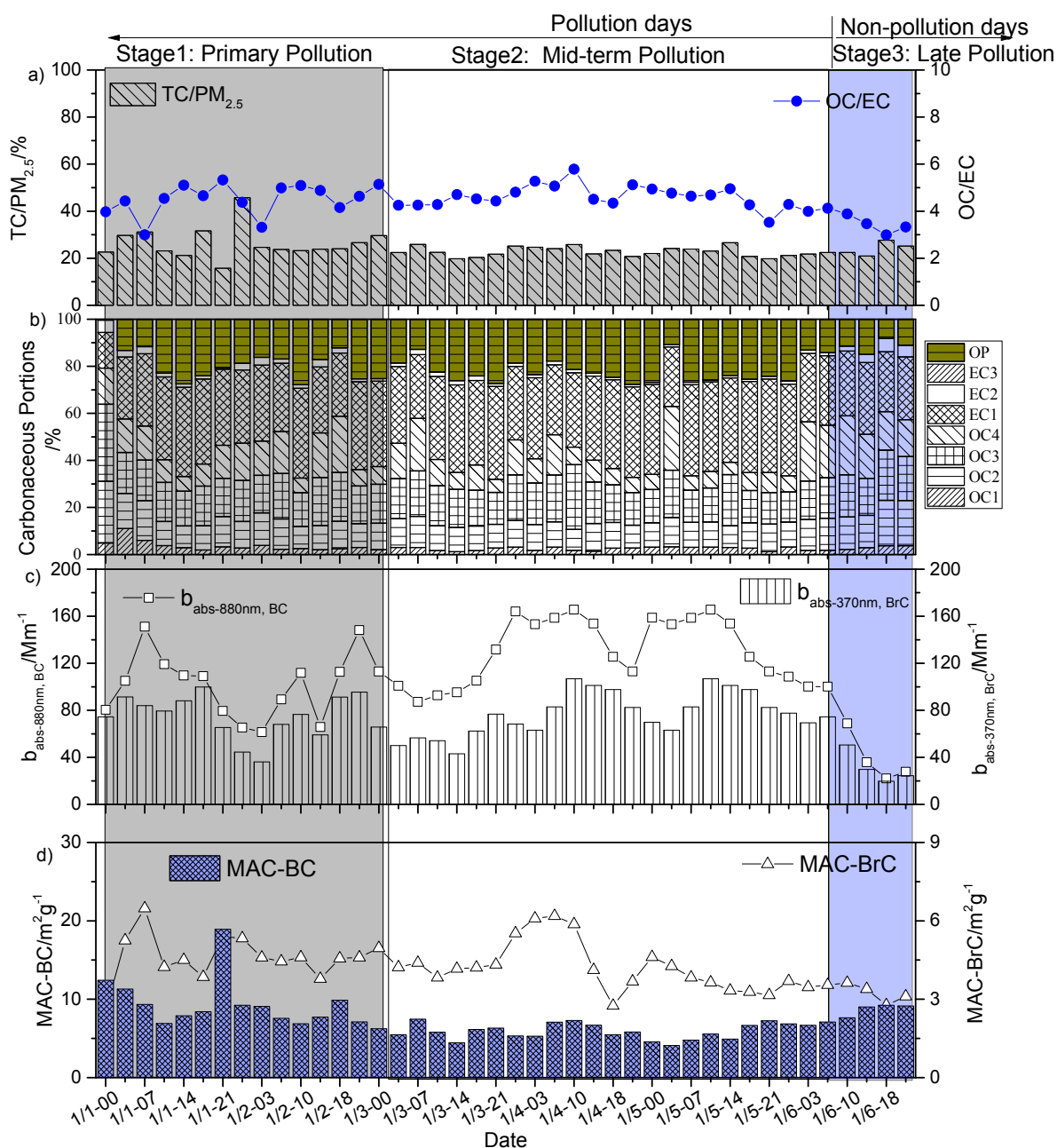
Fig. 5. Time series of (a) $TC/PM_{2.5}$ ratios (μg m^{-3}), (b) concentrations of major $PM_{2.5}$ carbon species, (c) $b_{abs-880nm, \, BC}$ and $b_{abs-370nm, \, BrC}$, and (d) MAC-BC and MAC-BrC during sampling days. Three colored regions represent the different pollution stages: primary pollution period, midterm pollution period, and late pollution period.

particles at 880 nm and the partial OAs of BrC, which can preferentially absorb light in near-ultraviolet and blue wavelengths (Andreae and Gelencsér, 2006; Habib *et al.*, 2008; Kirchstetter and Thatcher, 2012; Lei *et al.*, 2018). Since AAE is a highly sensitive approach to classify the presence of BrC, the average $AAE_{\_Full\ spectrum}$ values during pollution and non-pollution periods were 1.22 ± 0.02 and 1.30 ± 0.05, emphasizing the strong presence of BrC during our sampling periods in Xi'an. The average values of $b_{abs\text{-}880nm,\ BC}$ and $b_{abs\text{-}370nm,\ BrC}$ were 119.9 and 76.3 Mm^{-1} for pollution day $PM_{2.5}$ and 66.2 and 49.4 Mm^{-1} for non-pollution day PM_2, respectively (Fig. 5(c)). This illustrates the abundance of BC and BrC particles. The changes in $b_{abs\text{-}880nm,\ BC}$ experienced three periods. In the initial pollution period (January 1–2), the $b_{abs\text{-}880nm,\ BC}$ showed a large variability and peaked at the morning (07:00–10:00) and evening (18:00–21:00) rush hours, emphasizing that $b_{abs\text{-}880nm,\ BC}$ was more sensitive to traffic density at the beginning of the severe pollution. During the midterm pollution period of late January 3 to January 5, $b_{abs\text{-}880nm,\ BC}$ rose sharply on the morning of January 3 and then displayed relatively stable and high ranges (120–160 Mm^{-1}). These phenomena indicated that the high $b_{abs\text{-}880nm,\ BC}$ values during the second pollution period were mainly influenced by the accumulation of multiple primary sources (i.e., industrial, heating, and traffic emissions) under stable meteorological conditions and were less associated with the variations of traffic flow. The NO_2/SO_2 mixing ratio can be a useful tool to examine the relative contribution of vehicular sources. The emission ratio of NO_2 to SO_2 peaked at the high level of 3.5 on January 3 (primary pollution period) and decreased to 1.9 on January 5 (midterm pollution period), indicating that vehicle emissions and stationary sources both substantially contributed to severe pollution days. The increased accumulation from certain stationary sources in the middle of the pollution period contributed to the high $b_{abs\text{-}880nm,\ BC}$ (Han *et al.*, 2011; Tian *et al.*, 2016).

In comparison with $b_{abs\text{-}880nm,\ BC}$ values, the peaks of $b_{abs\text{-}370nm,\ BrC}$ mainly concentrated in the late-night period of 0:00–3:00 from January 1 to 3 and afternoon on pollution days. The afternoon peaks of $b_{abs\text{-}370nm,\ BrC}$ associated with increased $b_{abs\text{-}880nm,\ BC}$ values, primarily because of the accumulation of primary anthropogenic emissions during daytime. Therefore, residential coal and biomass burning were key contributors to heavy UV light-absorption. The midnight peaks of $b_{abs\text{-}370nm,\ BrC}$ stress that nighttime PM also contained strong UV absorption (Saleh *et al.*, 2013). Aqueous SOC formation in midnight during high RH condition should be one of important contributors for high $b_{abs\text{-}370nm,\ BrC}$. Previous literatures reported that the conditions of stagnant air, high RH, and low temperature in winter haze days also favored the partitioning of SVOCs to the particle phase through aqueous reactions (Strader *et al.*, 1999; Shrivastava *et al.*, 2008; Chen *et al.*, 2010). In addition, acidic aerosols also promote the formation of SOC. For instance, formation of high-molecular-weight (MW) SOC products has been observed during the OH-initiated oxidation of aqueous 3,5-dihydroxybenzoic acid (Kroll and Seinfeld, 2008); phenolic/methoxyphenols compounds forms

SOC via efficient OH addition to the aromatic ring from aqueous reactions (Sun *et al.*, 2010); and those of gaseous biomass precursors (isoprene and α-pinene) on acidic aerosol particles' (which involves sulfate radicals (SO_4^-)) surfaces (Limbeck, 2003; Noziere *et al.*, 2010; Perri *et al.*, 2010). Recent study by our group also revealed that one third of OC on average during haze days was formed through aqueous reactions under the high RH and stronger $PM_{2.5}$ acidity in Xi'an (Zhang *et al.*, 2015).

The MAC can be used to understand light-absorbing abilities. The MAC-BC values calculated at 880 nm using Eq. (2) were 15.3 and 11.2 $m^2\ g^{-1}$ for pollution and non-pollution days, respectively. The winter MAC-BC values exhibited wider variations, differing by a factor of up to four during sampling periods because of variable BC sources in winter. The MAC was not governed solely by absorbing efficiency; their sources also influenced it. Cheng *et al.* (2011) indicated that intensive biomass emissions reduce MAC-BC values; however, the abundant diesel exhaust during severe pollution days displayed relatively high MAC-BC values. Compared with the MAC-BC, the MAC-BrC (calculated at 370 nm in Eq. (1)) showed lower levels and less variability (2.2 $m^2\ g^{-1}$ for pollution PM and 2.4 $m^2\ g^{-1}$ for non-pollution PM). Thus, BrC is a weaker absorber than BC. A wide MAC-BrC range (Fig. 5(d); 1.2–2.8 $m^2\ g^{-1}$) covered ranges produced by regions with predominant biomass burning, such as Philadelphia (Jeong *et al.*, 2004) (2.4 $m^2\ g^{-1}$), Beijing (Cheng *et al.*, 2011) (0.71–1.79 $m^2\ g^{-1}$), and the Amazon basin (Hoffer *et al.*, 2006) (0.5–1.5 $m^2\ g^{-1}$) but was much higher compared with the traffic-dominated region of the southeastern United States (Bond, 2004) (0.31–0.70 $m^2\ g^{-1}$). As a result, these variations of MAC-BrC were possibly caused by the variety of fuel combustion sources during severe pollution periods.

CONCLUSION

The concentrations of gas pollutants (NO_2, SO_2, and CO), BC, and $PM_{2.5}$ were highest on pollution days and nearly double of those on non-pollution days. Based on SMPS analysis, both pollutive and non-polluting particles showed relatively large size ranges in this study and included the Aitken and accumulation modes. Diurnal variations of the pollutants' PN distribution emphasized the influences of fresh vehicle emissions and particle condensational growth. The condensation of much larger PM was observed in non-pollution periods. Among the carbon species, a considerable portion (approximately 60%) consisted of EC1, OC3, and OC4 on both non-pollution and pollution days, which emphasized the effect of coal burning during sampling days. Moreover, the high OC/EC (3.0–5.8) and SOC/TC (approximately 30%) ratios in this study indicated the noteworthy influence of SOC. The substantial OC2 and OC3 concentrations and high O_3 levels in the afternoon also support this conclusion. With regard to the light-absorbing properties, the diurnal pattern of $b_{abs\text{-}880nm,\ BC}$ showed different peak times during pollution days, strongly suggesting that BC was heavily influenced by traffic emissions in the early pollution period and

accumulated from other primary sources (i.e., heating and industrial emissions) in the midterm period. In contrast, the peaks of $b_{abs\text{-}370nm,\ BrC}$ corresponded to the periods of photochemical and aqueous SOC. The ranges of both MAC-BC and MAC-BrC vary noticeably, confirming that the dominant sources of BC and BrC change during a severe pollution period.

ACKNOWLEDGEMENTS

REFERENCES

Alexander, D.T., Crozier, P.A. and Anderson, J.R. (2008). Brown carbon spheres in east Asian outflow and their optical properties. *Science* 321: 833–836.

An, X., Hou, Q., Li, N. and Zhai, S. (2013). Assessment of human exposure level to PM_{10} in China. *Atmos. Environ.* 70: 376–386.

Andreae, M. and Gelencsér, A. (2006). Black carbon or brown carbon? The nature of light-absorbing carbonaceous aerosols. *Atmos. Chem. Phys.* 6: 3131–3148.

Bond, T.C. (2004). A technology-based global inventory of black and organic carbon emissions from combustion. *J. Geophys. Res.* 109: D14203.

Bond, T.C. and Bergstrom, R.W. (2006). Light absorption by carbonaceous particles: An investigative review. *Aerosol Sci. Technol.* 40: 27–67.

Bukowiecki, N., Kittelson, D., Watts, W., Burtscher, H., Weingartner, E. and Baltensperger, U. (2002). Real-time characterization of ultrafine and accumulation mode particles in ambient combustion aerosols. *J. Aerosol Sci.* 33: 1139–1154.

Cao, J.J., Wu, F., Chow, J.C. and Lee, S.C. (2005). Characterization and source apportionment of atmospheric organic and elemental carbon during fall and winter of 2003 in Xi'an, China. *Atmos. Chem. Phys.* 5: 3127–3137.

Cao, J.J., Lee, S.C., Chow, J.C., Watson, J.G., Ho, K.F., Zhang, R.J., Jin, Z.D., Shen, Z.X., Chen, G.C., Kang, Y.M., Zou, S.C., Zhang, L.Z., Qi, S.H., Dai, M.H., Cheng, Y. and Hu, K. (2007). Spatial and seasonal distributions of carbonaceous aerosols over China. *J. Geophys. Res.* 112: D22S11.

Chen, B.T., Schwegler-Berry, D., Cumpston, A., Cumpston, J., Friend, S., Stone, S. and Keane, M. (2016). Performance of a scanning mobility particle sizer in measuring diverse types of airborne nanoparticles: Multi-walled carbon nanotubes, welding fumes, and titanium dioxide spray. *J. Occup. Environ. Hyg.* 13: 501–518.

Chen, J., Ying, Q. and Kleeman, M.J. (2010). Source apportionment of wintertime secondary organic aerosol during the California regional $PM_{10}/PM_{2.5}$ air quality study. *Atmos. Environ.* 44: 1331–1340.

Cheng, Y., He, K.B., Zheng, M., Duan, F.K., Du, Z.Y., Ma, Y.L., Tan, J.H., Yang, F.M., Liu, J.M., Zhang, X.L., Weber, R.J., Bergin, M.H. and Russell, A.G. (2011). Mass absorption efficiency of elemental carbon and water-soluble organic carbon in Beijing, China. *Atmos. Chem. Phys.* 11: 11497–11510.

Cheng, Z., Wang, S., Jiang, J., Fu, Q., Chen, C., Xu, B., Yu, J., Fu, X. and Hao, J. (2013). Long-term trend of haze pollution and impact of particulate matter in the Yangtze River Delta, China. *Environ. Pollut.* 182: 101–110.

Chow, J.C., Watson, J.G., Louie, P.K., Chen, L.W. and Sin, D. (2005). Comparison of $PM_{2.5}$ carbon measurement methods in Hong Kong, China. *Environ. Pollut.* 137: 334–344.

Collaud Coen, M., Weingartner, E., Apituley, A., Ceburnis, D., Fierz-Schmidhauser, R., Flentje, H., Henzing, J., Jennings, S.G., Moerman, M. and Petzold, A. (2010). Minimizing light absorption measurement artifacts of the aethalometer: Evaluation of five correction algorithms. *Atmos. Meas. Tech.* 3: 457–474.

Dalirian, M., Ylisirniö, A., Buchholz, A., Schlesinger, D., Ström, J., Virtanen, A. and Riipinen, I. (2017). Cloud droplet activation of black carbon particles coated with organic compounds of varying solubility. *Atmos. Chem. Phys. Discuss., in Review.*

Fang, C., Zhang, Z., Jin, M., Zou, P. and Wang, J. (2017). Pollution characteristics of $PM_{2.5}$ aerosol during haze periods in Changchun, China. *Aerosol Air Qual. Res.* 17: 888–895.

Gao, J., Wang, T., Zhou, X., Wu, W. and Wang, W. (2009). Measurement of aerosol number size distributions in the Yangtze River Delta in China: Formation and growth of particles under polluted conditions. *Atmos. Environ.* 43: 829–836.

Gu, J., Bai, Z., Liu, A., Wu, L., Xie, Y., Li, W., Dong, H. and Zhang, X. (2010). Characterization of atmospheric organic carbon and element carbon of $PM_{2.5}$ and PM_{10} at Tianjin, China. *Aerosol Air Qual. Res.* 10: 167–176.

Guha, A., De, B.K., Dhar, P., Banik, T., Chakraborty, M., Roy, R., Choudhury, A., Gogoi, M.M., Babu, S.S. and Moorthy, K.K. (2015). Seasonal characteristics of aerosol black carbon in relation to long range transport over Tripura in Northeast India. *Aerosol Air Qual. Res.* 15: 786–798.

Habib, G., Venkataraman, C., Bond, T.C. and Schauer, J.J. (2008). Chemical, microphysical and optical properties of primary particles from the combustion of biomass fuels. *Environ. Sci. Technol.* 42: 8829–8834.

Han, S., Bian, H., Feng, Y., Liu, A., Li, X., Zeng, F. and Zhang, X. (2011). Analysis of the relationship between O_3, NO and NO_2 in Tianjin, China. *Aerosol Air Qual. Res.* 11: 128-139.

Hitchins, J., Morawska, L., Wolff, R. and Gilbert, D. (2000). Concentrations of submicrometre particles from vehicle emissions near a major road. *Atmos. Environ.* 34: 51–59.

Hoffer, A., Gelencsér, A., Guyon, P., Kiss, G., Schmid, O., Frank, G., Artaxo, P. and Andreae, M. (2006). Optical properties of humic-like substances (HULIS) in biomass-burning aerosols. *Atmos. Chem. Phys.* 6: 3563–3570.

Hyslop, N.P. (2009). Impaired visibility: The air pollution people see. *Atmos. Environ.* 43: 182–195.

Jeong, C.H., Hopke, P.K., Kim, E. and Lee, D.W. (2004). The comparison between thermal-optical transmittance elemental carbon and aethalometer black carbon measured at multiple monitoring sites. *Atmos. Environ.* 38: 5193–5204.

Ketzel, M., Wåhlin, P., Kristensson, A., Swietlicki, E., Berkowicz, R., Nielsen, O.J. and Palmgren, F. (2004). Particle size distribution and particle mass measurements at urban, near-city and rural level in the copenhagen area and southern Sweden. *Atmos. Chem. Phys.* 4: 281–292.

Kirchstetter, T.W. and Thatcher, T.L. (2012). Contribution of organic carbon to wood smoke particulate matter absorption of solar radiation. *Atmos. Chem. Phys.* 12: 6067–6072.

Kotzick, R. and Niessner, R. (1999). The effects of aging processes on critical supersaturation ratios of ultrafine carbon aerosols. *Atmos. Environ.* 33: 2669–2677.

Kroll, J.H. and Seinfeld, J.H. (2008). Chemistry of secondary organic aerosol: Formation and Evolution of low-volatility organics in the atmosphere. *Atmos. Environ.* 42: 3593–3624.

Law, K.S. and Stohl, A. (2007). Arctic air pollution: Origins and impacts. *Science* 315: 1537–1540.

Lei, Y., Shen, Z., Zhang, T., Zhang, Q., Wang, Q., Sun, J., Gong, X., Cao, J., Xu, H., Liu, S. and Yang, L. (2018). Optical source profiles of brown carbon in size-resolved particulate matter from typical domestic biofuel burning over Guanzhong plain, China. *Sci Total Environ.* 622: 244–251.

Levitt, N.P., Zhang, R., Xue, H. and Chen, J. (2007). Heterogeneous chemistry of organic acids on soot surfaces. *J. Phys. Chem. A* 111: 4804–4814.

Limbeck, A. (2003). Secondary organic aerosol formation in the atmosphere via heterogeneous reaction of gaseous isoprene on acidic Particles. *Geophys. Res. Lett.* 30: 1996.

Lin, C.C., Yang, L.S. and Cheng, Y.H. (2016). Ambient PM$_{2.5}$, black carbon, and particle size-resolved number concentrations and the Ångström exponent value of aerosols during the firework display at the lantern festival in southern Taiwan. *Aerosol Air Qual. Res.* 16: 373–387.

Liu, F. and Smallwood, G.J. (2011). The effect of particle aggregation on the absorption and emission properties of mono- and polydisperse soot aggregates. *Appl. Phys. B* 104: 343–355.

Liu, S., Hu, M., Wu, Z., Wehner, B., Wiedensohler, A. and Cheng, Y. (2008). Aerosol number size distribution and new particle formation at a rural/coastal site in Pearl River Delta (PRD) of China. *Atmos. Environ.* 42: 6275–6283.

Liu, X., Li, J., Qu, Y., Han, T., Hou, L., Gu, J., Chen, C., Yang, Y., Liu, X. and Yang, T. (2013). Formation and evolution mechanism of regional haze: A case study in

the megacity Beijing, China. *Atmos. Chem. Phys.* 13: 4501–4514.

Ma, J., Xu, X., Zhao, C. and Yan, P. (2012). A Review of atmospheric chemistry research in china: photochemical smog, haze pollution, and gas-aerosol interactions. *Adv. Atmos. Sci.* 29: 1006–1026.

Maricq, M.M. (2007). Chemical characterization of particulate emissions from diesel engines: A review. *J Aerosol Sci.* 38: 1079–1118.

Nel, A. (2005). Air pollution-related illness: Effects of particles. *Science* 308: 804–806.

Noziere, B., Ekstrom, S., Alsberg, T. and Holmstrom, S. (2010). Radical-initiated formation of organosulfates and Surfactants in Atmospheric Aerosols. *Geophys. Res. Lett.* 37: L05806.

Odman, M.T., Hu, Y., Russell, A.G., Hanedar, A., Boylan, J.W. and Brewer, P.F. (2009). Quantifying the sources of ozone, fine particulate matter, and regional haze in the southeastern United States. *J. Environ. Manage.* 90: 3155–3168.

Olson, M.R., Victoria Garcia, M., Robinson, M.A., Van Rooy, P., Dietenberger, M.A., Bergin, M. and Schauer, J.J. (2015). Investigation of black and brown carbon multiple-wavelength-dependent light absorption from biomass and fossil fuel combustion source emissions. *J. Geophys. Res.* 120: 6682–6697.

Peplow, M., Shen, H., Abbott, A., Morrison, J., Reardon, S., Mukerjee, M., Ledford, H., Gibney, E. and Callaway, E. (2014). Beijing smog contains witches' brew of microbes. *Nature* 505: 588.

Perez, N., Pey, J., Cusack, M., Reche, C., Querol, X., Alastuey, A., Viana, M. (2010). Variability of particle number, black carbon, and PM$_{10}$, PM$_{2.5}$, and PM$_1$ levels and speciation: Influence of road traffic emissions on urban air quality. *Aerosol Sci. Tech.* 44: 487–499.

Perri, M.J., Lim, Y.B., Seitzinger, S.P. and Turpin, B.J. (2010). Organosulfates from glycolaldehyde in aqueous aerosols and clouds: Laboratory studies. *Atmos. Environ.* 44: 2658–2664.

Polidori, A., Hu, S., Biswas, S., Delfino, R. and Sioutas, C. (2008). Real-time characterization of particle-bound polycyclic aromatic hydrocarbons in ambient aerosols and from motor-vehicle exhaust. *Atmos. Chemis. Phys.* 8: 1277–1291.

Pope III, C.A., Burnett, R.T., Thun, M.J., Calle, E.E., Krewski, D., Ito, K. and Thurston, G.D. (2002). Lung cancer, cardiopulmonary mortality, and long-term exposure to fine particulate air pollution. *JAMA* 287: 1132–1141.

Ramanathan, V. and Carmichael, G. (2008). Global and regional climate changes due to black carbon. *Nat. Geosci.* 1: 221–227.

Saleh, R., Hennigan, C.J., McMeeking, G.R., Chuang, W.K., Robinson, E.S., Coe, H., Donahue, N.M. and Robinson, A.L. (2013). Absorptivity of brown carbon in fresh and photo-chemically aged biomass-burning emissions. *Atmos. Chem. Phys.* 13: 7683–7693.

Sarkar, C., Chatterjee, A., Singh, A.K., Ghosh, S.K. and Raha, S. (2015). Characterization of black carbon aerosols over Darjeeling-A high altitude Himalayan station in

eastern India. *Aerosol Air Qual. Res.* 15: 465–478.

Shen, Z., Cao, J., Arimoto, R., Han, Z., Zhang, R., Han, Y., Liu, S., Okuda, T., Nakao, S. and Tanaka, S. (2009). Ionic composition of TSP and PM$_{2.5}$ during dust storms and air pollution episodes at Xi'an, China. *Atmos. Environ.* 43: 2911–2918.

Shen, Z., Cao, J., Arimoto, R., Han, Y., Zhu, C., Tian, J. and Liu, S. (2010). Chemical characteristics of fine particles (PM$_1$) from Xi'an, China. *Aerosol Sci. Technol.* 44: 461–472.

Shen, Z., Zhang, L., Cao, J., Tian, J., Liu, L., Wang, G., Zhao, Z., Wang, X., Zhang, R. and Liu, S. (2012). Chemical composition, sources, and deposition fluxes of water-soluble inorganic ions obtained from precipitation chemistry measurements collected at an urban site in northwest China. *J. Environ Monit.* 14: 3000–3008.

Shen, Z., Cao, J., Zhang, L., Liu, L., Zhang, Q., Li, J., Han, Y., Zhu, C., Zhao, Z. and Liu, S. (2014). Day-night differences and seasonal variations of chemical species in PM$_{10}$ over Xi'an, northwest China. *Environ. Sci. Pollu. Res. Int.* 21: 3697–3705.

Shen, Z., Cao, J., Zhang, L., Zhang, Q., Huang, R.J., Liu, S., Zhao, Z., Zhu, C., Lei, Y., Xu, H. and Zheng, C. (2016). Retrieving historical ambient PM$_{2.5}$ concentrations using existing visibility measurements in Xi'an, northwest China. *Atmos. Environ.* 126: 15–20.

Shen, Z., Zhang, Q., Cao, J., Zhang, L., Lei, Y., Huang, Y., Huang, R. J., Gao, J., Zhao, Z. and Zhu, C. (2017). Optical properties and possible sources of brown carbon in PM$_{2.5}$ over Xi'an, China. *Atmos. Environ.* 150: 322–330.

Shi, X., He, K., Zhang, J., Ma, Y., Ge, Y. and Tan, J. (2010). A comparative study of particle size distribution from two oxygenated fuels and diesel fuel. *Front. Environ. Sci. Eng. China* 4: 30–34.

Shrivastava, M.K., Lane, T.E., Donahue, N.M., Pandis, S.N. and Robinson, A.L. (2008). Effects of gas particle partitioning and aging of primary emissions on urban and regional organic aerosol concentrations. *J. Geophys. Res.* 113: D18301.

Strader, R., Lurmann, F. and Pandis, S.N. (1999). Evaluation of secondary organic aerosol formation in winter. *Atmos. Environ.* 33: 4849–4863.

Sun, Y.L., Zhang, Q., Anastasio, C. and Sun, J., (2010). Insights into secondary organic aerosol formed via aqueous-phase reactions of phenolic compounds based on high resolution mass spectrometry. *Atmos. Chem. Phys.* 10: 4809–4822.

Tan, J.H., Duan, J.C., Chen, D.H., Wang, X.H., Guo, S.J., Bi, X.H., Sheng, G.Y., He, K.B. and Fu, J.M. (2009). Chemical characteristics of haze during summer and winter in Guangzhou. *Atmos. Res.* 94: 238–245.

Tian, M., Wang, H., Chen, Y., Yang, F., Zhang, X., Zou, Q., Zhang, R., Ma, Y. and He, K. (2016). Characteristics of aerosol pollution during heavy haze events in Suzhou, China. *Atmos. Chem. Phys.* 16: 7357–7371.

Tian, S., Pan, Y., Liu, Z., Wen, T. and Wang, Y. (2014). Size-resolved aerosol chemical analysis of extreme haze pollution events during early 2013 in urban Beijing,

China. *J. Hazard. Mater.* 279: 452–460.

Turpin, B.J. and Huntzicker, J.J. (1995). Identification of secondary organic aerosol episodes and quantitation of primary and secondary organic aerosol concentrations during SCAQS. *Atmos. Environ.* 29: 3527–3544.

Van Gulijk, C., Marijnissen, J.C.M., Makkee, M., Moulijn, J.A. and Schmidt-Ott, A. (2004). Measuring diesel soot with a scanning mobility particle sizer and an electrical low-pressure impactor: Performance assessment with a model for fractal-like agglomerates. *J. Aerosol Sci.* 35: 633–655.

Von Schneidemesser, E., Monks, P.S., Allan, J.D., Bruhwiler, L., Forster, P., Fowler, D., Lauer, A., Morgan, W.T., Paasonen, P. and Righi, M. (2015). Chemistry and the linkages between air quality and climate change. *Chem. Rev.* 115: 3856–3897.

Wang, X., Shen, Z., Cao, J., Zhang, L., Liu, L., Li, J., Liu, S. and Sun, Y. (2012). Characteristics of surface ozone at an urban site of Xi'an in northwest China. *J. Environ. Monit.* 14: 116–126.

Wentzel, M., Gorzawski, H., Naumann, K.H., Saathoff, H. and Weinbruch, S. (2003). Transmission electron microscopical and aerosol dynamical characterization of soot aerosols. *J. Aerosol Sci.* 34: 1347–1370.

Winkler, P. (1973). The growth of atmospheric aerosol particles as a function of the relative humidity—II. An improved concept of mixed nuclei. *J. Aerosol Sci.* 4: 373–387.

Yang, Y., Liu, X., Qu, Y., Wang, J., An, J., Zhang, Y. and Zhang, F. (2015). Formation Mechanism of continuous extreme haze episodes in the megacity Beijing, China, in January 2013. *Atmos. Res.* 155: 192–203.

Yue, D., Zhong, L., Zhang, T., Shen, J., Yuan, L., Ye, S., Zhou, Y. and Zeng, L. (2016). Particle growth and variation of cloud condensation nucleus activity on polluted days with new particle formation: A case study for regional air pollution in the PRD region, China. *Aerosol Air Qual. Res.* 16: 323–335.

Zhan, C., Zhang, J., Cao, J., Han, Y., Wang, P., Zheng, J., Yao, R., Liu, H., Li, H. and Xiao, W. (2016). Characteristics and sources of black carbon in atmospheric dustfall particles from Huangshi, China. *Aerosol Air Qual. Res.* 16: 2096–2106.

Zhang, K.M. and Wexler, A.S. (2004). Evolution of particle number distribution near roadways-Part I: Analysis of aerosol dynamics and its implications for engine emission measurement. *Atmos. Environ.* 38: 6643–6653.

Zhang, K.M., Wexler, A.S., Zhu, Y.F., Hinds, W.C. and Sioutas, C. (2004). Evolution of particle number distribution near roadways. Part II: The 'Road-to-Ambient' process. *Atmos. Environ.* 38: 6655–6665.

Zhang, Q., Shen, Z., Cao, J., Zhang, R., Zhang, L., Huang, R.J., Zheng, C., Wang, L., Liu, S. and Xu, H. (2015). Variations in PM$_{2.5}$, BC and trace gases (NO$_2$, SO$_2$, and O$_3$) between haze and non-haze episodes in winter over Xi'an, China. *Atmos.Environ.* 112: 64–71.

Zhang, Q., Ning, Z., Shen, Z., Li, G., Zhang, J., Lei, Y., Xu, H., Sun, J., Zhang, L. and Westerdahl, D. (2017).

Variations of Aerosol size distribution, chemical composition and optical properties from roadside to ambient environment: A Case Study in Hong Kong, China. *Atmos. Environ.* 150: 322–330.

Zheng, G.J., Duan, F.K., Su, H., Ma, Y.L., Cheng, Y., Zheng, B., Zhang, Q., Huang, T., Kimoto, T., Chang, D., Pöschl, U., Cheng, Y.F. and He, K.B. (2015). Exploring the severe winter haze in Beijing: The impact of synoptic weather, regional transport and heterogeneous reactions. *Atmos. Chem. Phys.* 15: 2969–2983.

Zhou, B., Wang, Q., Zhou, Q., Zhang, Z., Wang, G., Fang, N., Li, M. and Cao, J. (2018). Seasonal characteristics of black carbon aerosol and its potential source regions in Baoji, China. *Aerosol Air Qual. Res.* 18: 397–406.